Surfactants Used in Colloidal Synthesis Modulate Ni Nanoparticle Surface Evolution for Selective CO_2 Hydrogenation

Xiangru Wei[#], Grayson Johnson[#], Yifan Ye[*], Meiyang Cui, Shen-Wei Yu, Yihua Ran, Jun Cai, Zhi Liu, Xi Chen, Wenpei Gao, Ethan J. Crumlin, Xu Zhang, Robert J. Davis, Zhangxiong Wu[*], Sen Zhang[*]

ABSTRACT: Colloidal chemistry holds promise to prepare uniform and size-controllable pre-catalysts; however, it remains a challenge to unveil the atomic level transition from pre-catalyst to active catalytic surfaces under the reaction conditions to enable the mechanistic design of catalysts. Here we report an ambient pressure X-ray photoelectron spectroscopy (AP-XPS) study, coupled with operando environmental transmission electron microscopy, infrared spectroscopy, and theoretical calculations, to elucidate the surface catalytic sites of colloidal Ni nanoparticles for CO_2 hydrogenation. We show that Ni nanoparticles with phosphine ligands exhibit a distinct surface evolution compared with amine-capped ones, owing to the diffusion of P under oxidative (air) or reductive (CO_2 + H_2) gaseous environments at elevated temperatures. The resulting NiP_x surface leads to a substantially improved selectivity for CO production, in contrast to the metallic Ni, which favors CH_4. The further elimination of metallic Ni sites by designing multi-step P incorporation, observed via operando probes, achieves unit selectivity of CO in high-rate CO_2 hydrogenation.

INTRODUCTION

Solutions to climate change and energy sustainability of modern society require the efficient management of carbon-based fuels and chemicals.[1-3] Designating CO_2, one of the major greenhouse gases, as a carbon feedstock to produce commodity chemicals has garnered enormous interest, as it would provide an alternative to non-renewable petrochemical sources.[4,5] Coupled with renewable H_2 and energy sources, heterogeneous catalytic CO_2 hydrogenation is a promising approach to closing the loop of carbon emission.[6,7] Under atmospheric pressure, CO is one of the most appealing products from CO_2 hydrogenation via the reverse water–gas shift reaction (RWGS, $CO_2 + H_2 \rightarrow CO + H_2O$), given its versatile role in the production of liquid hydrocarbons and oxygenates through well-established gas conversion technologies (e.g., Fischer–Tropsch synthesis and methanol synthesis).[8,9] However, the RWGS conversion is often accompanied by the methanation reaction ($CO_2 + 4H_2 \rightarrow CH_4 + 2H_2O$), which generates lower-value, gaseous CH_4, making the selectivity control a central challenge of atmospheric CO_2 hydrogenation processes with minimized downstream separation cost.[10-12]

At the core of rational catalyst design for the CO_2 hydrogenation is the atomic-level understanding of catalyst structure-property relationships. Previous theoretical and experimental studies suggested that adsorbed CO (*CO) is a key intermediate in CO_2 hydrogenation, and its strong binding often allows the subsequent methanation to produce CH_4.[11,13,14] Guided by this principle, the synthetic tuning of metal nanoparticle sizes,[15] alloy compositions,[16,17] and metal-support interactions,[18-21] has been studied to improve the selectivity for CO production. For example, scaling down Ru and Pd nanoparticles to the single atom regime can suppress the CO_2 methanation.[22-24] Despite enormous efforts, it is still rare to achieve unity selectivity of CO with high-rate conversion of CO_2.

Another obstacle to the mechanistic understanding of heterogeneous catalysis is the structural complexity of many catalysts.[25] Recent advances in colloidal chemistry have allowed us to prepare monodisperse nanoparticles with well-defined surfaces and structures that are employed as simplified model systems.[26-31] But these well-defined nanoparticle catalysts may involve surface structure evolutions sensitive to the post-treatments (e.g., the removal of surfactants through thermal annealing) and catalytic conditions. Therefore, *in-situ*/*operando* characterizations are required to bridge the knowledge gap between as-synthesized nanoparticle pre-catalysts and the real catalytic structures. For example, we used ambient-pressure X-ray photoelectron spectroscopy (AP-XPS) and environmental transmission electron microscopy (TEM) to probe a catalyst under reactant gases and uncovered the structural transition of monodisperse CoPd alloy nanoparticles to Pd-CoO_x quasi-core/shell structures under CO oxidation conditions.[32] We envision that such a multimodal, *in-situ*/*operando* investigation will provide unprecedented opportunities to elucidate the catalytic structures for active CO_2 hydrogenation catalysts.

This article highlights the significant impact of capping ligands on colloidal Ni nanoparticle surface evolution and reconstruction in CO_2 hydrogenation. Ni is a well-known catalyst for the CO_2 methanation reaction.[33, 35, 36] Our studies using colloidal Ni nanoparticles with different capping ligands reveal that switching from amine (oleylamine) to phosphine (tributylphosphine or trioctylphosphine) ligands results in a drastic product selectivity change from CH_4 to CO under the same CO_2 hydrogenation conditions. Using AP-XPS and *operando* environmental TEM, the surface evolution landscapes of the catalysts are identified under different gas conditions and temperatures. As illustrated in **Fig. 1**, in contrast to amine-capped Ni that provides conventional

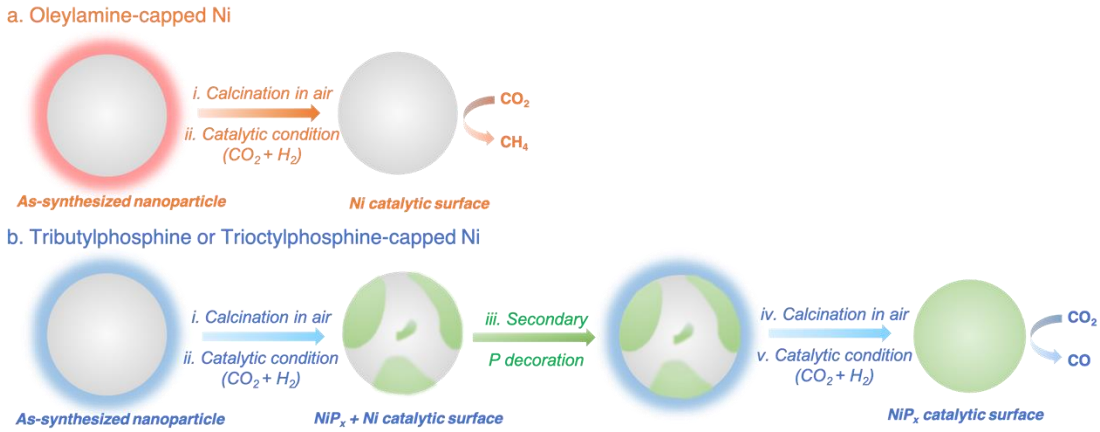

Figure 1. Schematic illustration of capping ligand governed Ni nanoparticle surface evolution. **a**, Oleylamine (OAm)-capped Ni nanoparticles provide a catalytic surface of metallic Ni after a calcination in air (to remove the bulky surfactant) and a reduction under CO_2 hydrogenation conditions. **b**, Phosphine (TOP or TBP)-capped Ni nanoparticles present a transition to generate a NiP_x dominant surface, and the metallic Ni site can be completely removed via a secondary phosphine treatment.

metallic Ni sites for CO_2 methanation, we find that phosphine-capped Ni undergoes an evident, partial transition to NiP_x under catalytic conditions, which suppresses metallic Ni surface sites and delivers a selective CO production (60-90% depending on the size of Ni nanoparticles). Furthermore, secondary phosphine modification of the Ni catalyst makes it possible to completely eliminate the metallic Ni species, leading to a unit selectivity of CO (100%) with high reaction rate and durability. Density functional theory (DFT) calculations and *operando* diffuse reflectance infrared Fourier transform spectroscopy (DRIFTs) validate that the NiP_x surface is beneficial to the selective CO production through the weakened *CO binding strength.

RESULTS AND DISCUSSION

Synthesis and Characterization of As-Synthesized Ni Nanoparticles. Ni nanoparticles capped with amine or phosphine ligands were synthesized by the reduction of nickel acetylacetonate ($Ni(acac)_2$) in the presence of OAm or TBP surfactants, according to the reported colloidal methods.[34, 35] The obtained nanoparticles are labeled as Ni-4.2 and Ni-P-4.2, and both are highly uniform with an average size of 4.2 ± 0.4 nm as shown in the TEM images in **Fig. 2a** and **Fig. S1**. By using the bulkier ligand, TOP, instead of TBP, the sizes of Ni-P were tuned to be 8.7 ± 0.4 (Ni-P-8.7), and 12.0 ± 0.5 nm (Ni-P-12), as indicated in **Fig. S2**. The TOP functions to decrease the number of nuclei in the colloidal synthesis, allowing more atoms to be used in the particle growth to form larger nanoparticles, which is consistent with our previous report.[34] For the subsequent catalytic testing, all as-synthesized nanoparticles were loaded onto commercial TiO_2 (P25) powders through sonication-assisted physical adsorption, with the Ni metal loading ratio controlled to be 2 wt.% (confirmed with inductively coupled plasma-optical emission spectrometer (ICP-OES)).

Catalytic Performance of Nanoparticles in CO_2 Hydrogenation. The TiO_2-supported Ni and Ni-P nanoparticles were pretreated in air at 400 °C to remove the organic ligands. The calcination in an oxidative gas environment has been widely used to remove surfactants with long hydrocarbon chains for colloidal nanocatalysts, but often causes surface oxidation of nanoparticles. The calcined samples were subsequently annealed in reductive gas conditions (1 vol.% CO_2 + 4 vol.% H_2 + 95 vol.% N_2, same as the CO_2 hydrogenation experimental conditions) at 400 °C to activate the nanoparticle surface for catalytic reactions {Experimental section in Supporting Information (SI)}. The TEM image in **Fig. 2b** confirms that the supported nanoparticles well preserve their sizes and morphologies after the pretreatment. For the Ni-P sample after calcination, we can confirm its amorphous structure based on aberration corrected scanning TEM high-angle annular dark field (STEM HAADF) images (**Fig. S3**). We also used STEM electron energy loss spectroscopy (STEM EELS) to analyze the Ni-P sample after the calcination, which clearly indicates incorporation and homogeneous distribution of P in the treated sample (**Fig. 2c**).

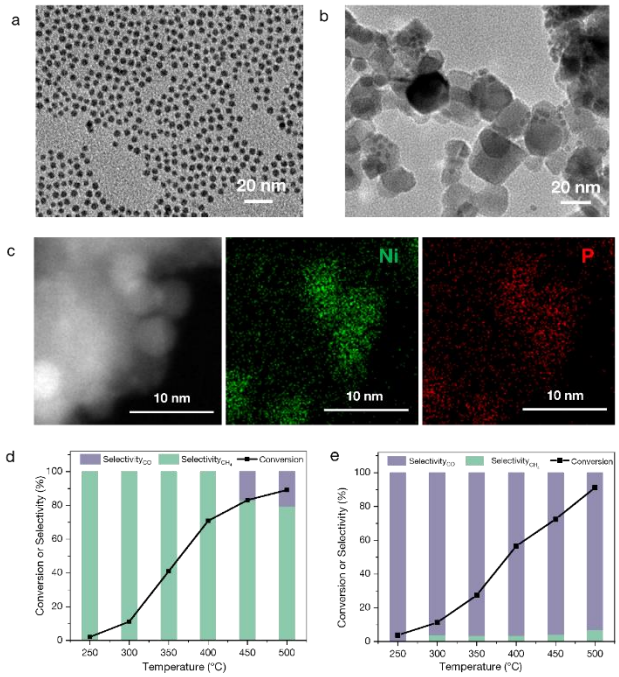

Figure 2. (**a**, **b**) TEM images of as-synthesized Ni-P-4.2 nanoparticles (a) and TiO_2-supported Ni-P-4.2 after calcination (b). (**c**) STEM HAADF image and EELS mapping of the TiO_2-supported Ni-P-4.2 after calcination. (**d, e**) Catalytic performances of the TiO_2-supported Ni-4.2 (d) and Ni-P-4.2 (e) catalysts for CO_2 hydrogenation as a function of temperature (1 vol.% CO_2 + 4 vol.% H_2 + 95 vol.% N_2 with a space velocity of ~30,000 mL g_{cat}^{-1} h^{-1} at ambient pressure).

Fig. 2d and **2e** summarize the catalytic performance of Ni-4.2 and Ni-P-4.2 for ambient-pressure CO_2 hydrogenation. The Ni-4.2 exhibits a typical methanation catalyst behavior,[36,37] with CO_2 being completely converted into CH_4 at temperatures lower than 400 °C. Although high temperature is known to favor CO production, the CO selectivity over Ni-4.2 catalyst is still lower than 30% at 500 °C. A significantly improved selectivity towards CO was observed on Ni-P-4.2 catalysts, which was consistently in the range of 90-93% at 250-500 °C. The Ni-P-4.2 catalyst delivers a high conversion of CO_2 at 55.5% at 400 °C. Moreover, there is little product selectivity change for both Ni-4.2 and Ni-P-4.2 catalysts when the CO_2 conversion is lowered by tuning the feed gas space velocity and reaction temperature (**Fig. S4** and **S5**). Based on the kinetic measurements, we observed a lower apparent activation energy (E_a) for CO productionon the Ni-P-4.2 (36.2 ± 1.1 kJ mol^{-1}) than Ni-4.2 catalyst (82.6 ± 1.4 kJ mol^{-1}) for CO_2 methanation (**Fig. S6**).[38] These results suggest that the Ni and Ni-P provide distinct catalytic sites, which enables the selectivity modulation of CO_2 hydrogenation product.

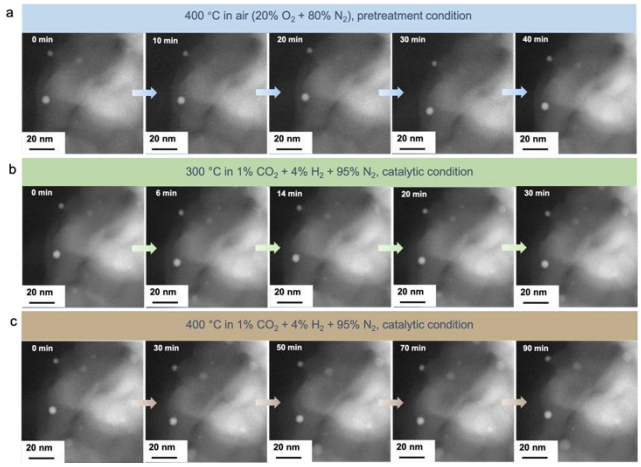

Figure 3. *Operando* observation of the structures of Ni-P-4.2 nanoparticles supported on TiO_2 during the pretreatment and the catalytic reactions. TEM images collected at (**a**) 400 °C in air (20 vol.% O_2 + 80 vol.% N_2) for 40 minutes, (**b**) 300 °C in reductive environment (1 vol.% CO_2 + 4 vol.% H_2 + 95 vol.% N_2) for 30 minutes, and (**c**) 400 °C in reductive environment (1 vol.% CO_2 + 4 vol.% H_2 + 95 vol.% N_2) for 90 minutes.

***Operando* environmental TEM characterization.** To unveil the possible nanoparticle size, morphology, and dispersity changes during the reaction, we carried out *operando* environmental TEM measurement on TiO_2-supported Ni-P-4.2 nanoparticles with a gas cell simulating both the pretreatment and catalytic conditions (**SI**). As shown in **Fig. 3**, the Ni-P nanoparticles can be readily distinguished from the TiO_2 support due to their Z contrast difference. Although the gas-cell configuration and heating-induced sample shifting limit the environmental TEM resolution, it is evident that nanoparticle size, morphology, and dispersity are well maintained at the elevated temperatures, regardless of the oxidative or reductive conditions. It is further corroborated by *ex-situ* TEM images of the used catalyst in **Fig. S7a**. In addition, the STEM HAADF image indicates that the used Ni-P catalysts preserve their amorphous nanoparticle structure (**Fig. S7b**). Previous studies reported that metallic nanoparticles, such as Ru, can be disintegrated into single atoms or clusters due to strong metal-support interactions, which promote the CO selectivity in CO_2 hydrogenation.[15] Our *operando* and *ex-situ* TEM studies enable us to exclude size and morphology changes in our catalytic materials, and indeed motivate us to further reveal the molecular-level active surface sites for Ni-P catalysts using AP-XPS.

Surface evolution of Ni-P nanoparticles under the pretreatment and catalytic conditions. The as-synthesized Ni-P-4.2 shows an intense C 1s XPS signal originating from the surfactant layer on the nanoparticles (**Fig. S8**). It also presents metallic Ni $2p_{3/2}$ (at binding energy BE = 852.6 eV) and P $2p_{3/2}$ (BE = 129.3 eV) peaks (**Fig. 4a**).[39,40] An additional P 2p signal at 132.1 eV is assigned to the oxidized phosphine ligands attached on the nanoparticle surface.[41] To elucidate the surface evolution of catalyst, we monitored the Ni-P-4.2 AP-XPS spectra while exposing the sample in a sequence of different gaseous environments that mimic the pretreatment (0.1 mbar of O_2 and 0.4 mbar of N_2 at 400 °C) and reaction conditions (0.1 mbar of CO_2 and 0.4 mbar of H_2 at 100 °C, 200 °C, 300 °C, and 400 °C). There is almost no C signal that can be detected after the pretreatment, indicating the hydrocarbon chain of organic ligand is decomposed and removed (**Fig. S8**). The oxidative pretreatment leads to the dominant NiO surface in the Ni-P sample, evidenced by NiO fingerprint signals at 853.7 eV in the Ni 2p spectrum and at 529.1 eV in the O 1s spectrum (**Fig. 4a**).[42] It is worth noting that the P 2p signal vanishes after the pretreatment, also confirming the surface dominance of NiO. Such a NiO surface is maintained in the CO_2 hydrogenation reaction gases at low temperatures (100 °C and 200 °C).

Once treating the sample in the CO_2 hydrogenation reaction gases at 300 °C, the NiO surface is reduced, as indicated by the downshift of Ni 2p peak to 852.6 eV and the disappearance of the O 1s peak at 529 eV (**Fig. 4a**). Interestingly, we observed that the Ni 2p at this condition showed a satellite peak with BE ~ 6.2 eV higher, which is clearly larger than that of the metallic Ni (~ 5.7 eV). It is established that NiP_x often presents an indistinguishable Ni 2p main peak with metallic Ni, but its satellite features are sensitive to P content in NiP_x.[43] Therefore, the Ni-P-4.2 surface species under CO_2 hydrogenation reaction is primarily NiP_x rather than metallic Ni. It is also confirmed by the re-emergence of P 2p signals at elevated temperatures, with two peaks corresponding to NiP_x and PO_x species. The P 2p signal intensity is further increased at 400 °C, demonstrating the further enrichment of P content on the surface.

The surface structure under different conditions is associated with the robustness of P against ligand removal in the calcination, and its migration and redistribution within the Ni-P nanoparticles. This process produces the NiP_x surface in the reductive gas condition of CO_2 hydrogenation, which probably underpins the distinct catalytic property

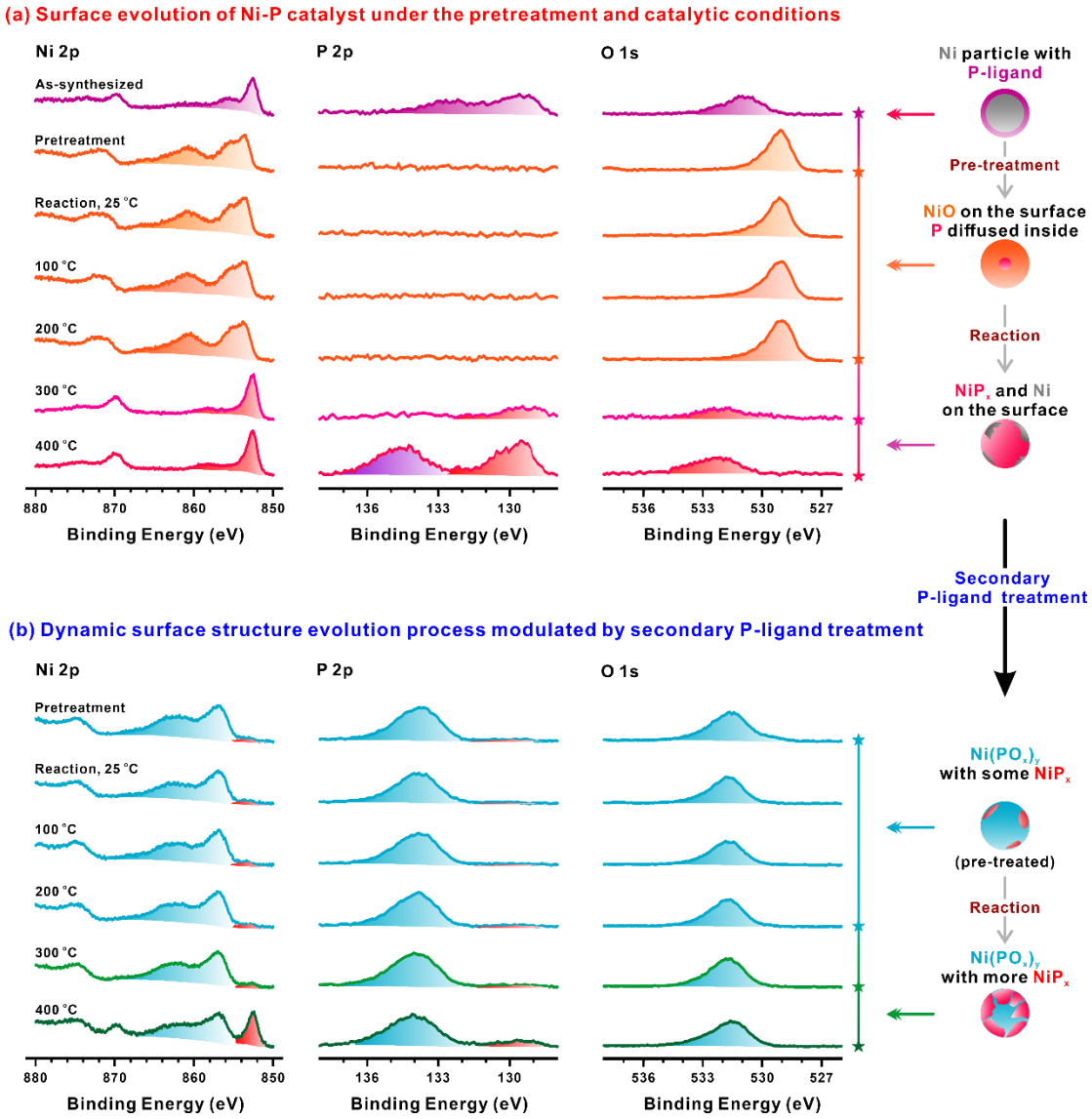

Figure 4. Surface evolution of Ni-P nanoparticles. a, b, AP-XPS measurements of the Ni-P-4.2 nanoparticles in different conditions from as-synthesized Ni-P-4.2 catalyst (a) and secondary P-treated catalyst (b). Ni 2p, P 2p and O 1s spectra were obtained under 0.5 mbar of mixtures of O_2 and N_2, or under 0.1 mbar of CO_2 and 0.4 mbar of H_2, at different temperatures. The spectra were acquired in normal emission geometry using a monochromated Al Kα emission source (hν = 1486.6 eV).

compared to metallic Ni. While the NiP_x is proposed as the active catalytic species for CO production, we still observed a certain portion of CH_4 in the product (7-10%) over Ni-P-4.2 catalyst. Considering that P is solely from the phosphine ligand bound to the nanoparticle, we hypothesize that such a monolayer P source cannot completely remove the surface metallic Ni sites in the catalyst, causing the undesirable methanation reaction. This point was corroborated by using Ni-P-8.7 and Ni-P-12 nanoparticles. With a larger size, the P source from the monolayer of phosphine ligands becomes further inadequate in the metal phosphorization. As a result, the CO selectivity decreases to 78.5% and 68.8% for Ni-P-8.7 and Ni-P-12 catalysts, respectively (**Table. S1**).

Secondary P modification to optimize the catalyst selectivity. The used Ni-P catalyst was stirred in the solution of TOP (1 mM in ethanol) to allow for the secondary phosphine ligand binding. Followed by the similar treatment (calcination in air to remove organic hydrocarbon and then in reductive gas), the secondary P incorporation was designed to phosphorize the remaining surface metallic Ni, as described in **Fig.4b**. The resulting Ni-P catalysts showed a 100% selectivity for the CO product (**Fig. 5a**). Even for Ni-P-12, CH_4 was completely undetectable, which confirmed the efficacy of secondary P incorporation. We also found that the obtained catalyst was highly durable. With a 65% conversion of CO_2 and a 100% selectivity for CO product, the Ni-P-4.2 exhibits a CO production rate of 28 mmol g_{cat}^{-1} h^{-1} at 400 °C and well maintains the performance in a 150-hour stability test (**Fig. 5b**).

Fig. 4b summarizes the AP-XPS spectra of the Ni-P-4.2 sample related to secondary P modification process. A major change we observed in the oxidative conditions at 400 °C is that Ni 2p signal is at 857 eV, which is clearly different from the original Ni-P-4.2 sample (BE = 852.6 eV).[44] Meanwhile,

the NiP_x peak in the P 2p spectra substantially attenuates, while a strong PO_x signal is detected. The O 1s spectrum shows a peak at BE 531.7 eV, much higher than that of NiO. These changes clearly demonstrate that the surface is dominated by $Ni(PO_x)_y$ species rather than NiO, after the secondary P incorporation. The excess amount of P enables the effective metal phosphorization that couples with the oxidation process to generate $Ni(PO_x)_y$. It is also found that the oxidized sample still has a small proportion of NiP_x on the surface, with weak peaks at lower BE regions on both Ni 2p and P 2p spectra. Bypassing the NiO formation, the secondary P treated Ni-P-4.2 sample displays unaltered spectra under reductive CO_2 hydrogenation condition from room temperature to 300 °C. The transformation from $Ni(PO_x)_y$ to NiP_x can be observed at 400 °C, which generates more active sites for CO_2-to-CO selective conversion. The direct comparison of the APXPS spectra of Ni-P catalyst before and after secondary P modification allows us to conclude that the incorporation of P, left by phosphine ligand decomposition, is the cornerstone to minimize the metallic Ni sites and thus to optimize CO product selectivity.

The role of NiP_x catalytic sites. *Operando* DRIFTS was used to understand the CO_2 hydrogenation pathways over Ni and Ni-P catalysts under flow reaction conditions. Once the model reaction gas (2 vol.% CO_2 + 8 vol.% H_2 + 90 vol.% N_2) is fed into the cell at room temperature, both Ni and Ni-P catalysts display the characteristic bands of bicarbonate (1381, and 1689 cm^{-1}) that results from the reaction between CO_2 and the hydroxyl group on the TiO_2 support (**Fig. 5c** and **5d**).[45] The bicarbonate peak intensity gradually decreases along with the rise of temperature, while new peaks attributed to adsorbed formate species appear at 2980 and 2939 cm^{-1}.[16] Formate has been claimed as a possible intermediate for CO_2 methanation in previous reports.[11,46] The similar feature of bicarbonate-to-formate transition on our Ni and Ni-P catalysts suggests that formate is an intermediate for both CO and CH_4 formation, but not the key to determine the catalyst selectivity. Most interestingly, we found a very different CO adsorption behavior over the Ni and Ni-P catalysts. On Ni, a peak at 1845 cm^{-1} is detected at 300 °C, which is correlated with multi-centered *CO on multifold hollow Ni sites (**Fig. 5c**).[11] This multi-centered *CO band is accompanied by a gaseous CH_4 peak (at 3017 cm^{-1}) whose intensity increases with the temperature.[20] In contrast to the Ni catalyst, the primary *CO on Ni-P is linear *CO on the atop site with a stretching band at 2,071 cm^{-1} (**Fig. 5d**).[19] In addition, the adsorbed CO molecules diffusing from the Ni to the Ti sites can be identified at 2168 cm^{-1} at 400 °C for Ni-P catalyst, but the gaseous CH_4 peak is negligible.[47,48]

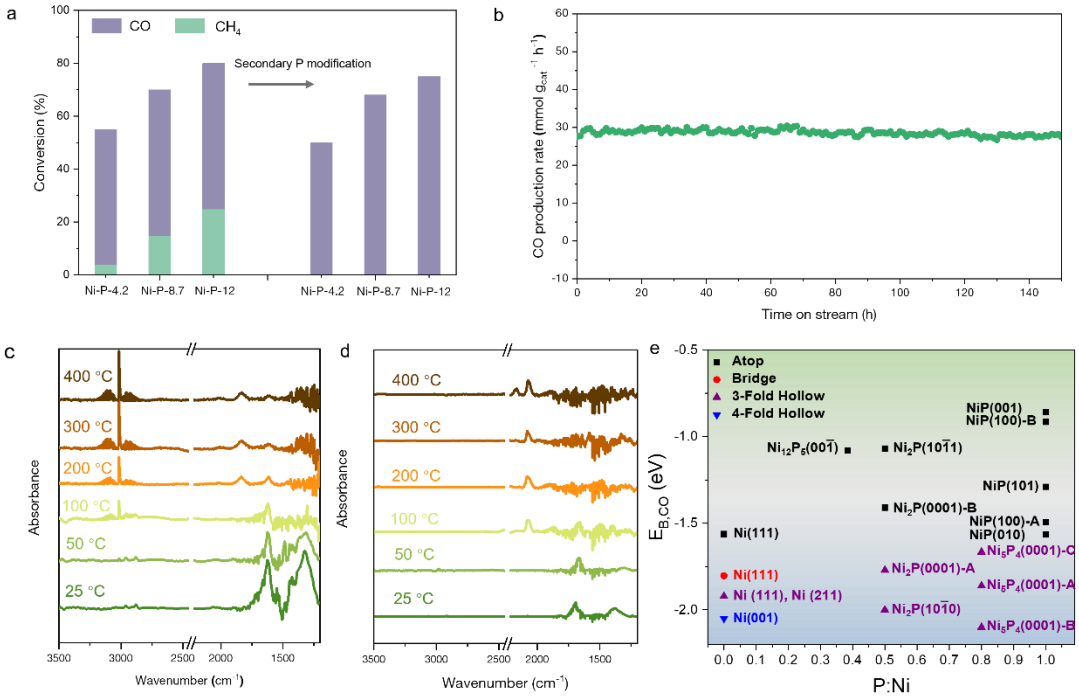

Figure 5. Catalytic performance and the NiP_x site properties. a, comparison of activity and selectivity on various catalysts before and after secondary P modification (1 vol.% CO_2 + 4 vol.% H_2 + 95 vol.% N_2 at ambient pressure, 400 °C). **b**, catalytic stability of secondary P modified Ni-P-4.2 (1 vol.% CO_2 + 4 vol.% H_2 + 95 vol.% N_2 at ambient pressure, 400 °C). **c, d**, *Operando* DRIFT spectra following exposure to feeding gas at 50 °C and subsequent stepwise heating to 400 °C under the same flow for Ni-4.2 (c) and Ni-P-4.2 (d). **e**, DFT calculation results of CO binding energies on Ni and various NiP_x surfaces.

We also investigated the *CO binding strength on Ni and Ni-P catalysts by using temperature-programmed desorption (TPD) DRIFTS. The CO-saturated samples were flushed with Ar under a series of temperatures with TPD DRIFTS spectra being recorded. As shown in **Fig. S9**, Ni-P showed a complete CO desorption at room temperature. The multi-centered *CO is much more stable and still present on the surface of Ni at 450 °C and 500 °C. Based on these results, it is clear that Ni-P catalyst can effectively decrease the binding strength of *CO by diminishing multi-centered CO

adsorption. It is also in an excellent agreement with the catalytic performance of Ni and Ni-P catalysts; i.e., Ni-P is favorable for the CO desorption and avoids the deep hydrogenation (methanation) to produce CH_4.

DFT simulations demonstrate that the P incorporation in Ni effectively alters the CO binding energy ($E_{B,CO}$). Given the fact that our Ni-P catalyst has an amorphous structure, we simulated a series of Ni-P surfaces, including Ni_2P (0001)-(2 terminations, A and B), Ni_2P ($10\bar{1}0$), Ni_2P ($10\bar{1}1$), Ni_5P_4 (0001)-(3 terminations, A, B, and C), NiP (001)-(2 terminations, A and B), NiP (010), NiP (100), NiP (101), and $Ni_{12}P_5$ ($00\bar{1}$) surfaces, to encompass possible adsorption sites for CO. These results were compared to the CO adsorption models on the Ni (001), Ni (111), and Ni (211) surfaces. $E_{B,CO}$ for the most stable adsorption site is aggregated in **Fig. 5e** against the P:Ni ratio and tabulated in **Table S2**. CO adsorption on Ni surfaces is strongest in the hollow sites with binding energies of -2.05 eV, -1.92 eV, and -1.92 eV on Ni (001), (111), and (211) respectively, which are consistent with previous DFT calculations.[49-52] After the P is incorporated, the $E_{B,CO}$ is strongly surface dependent, varying from -2.05 eV on Ni_5P_4 ($000\bar{1}$) to -0.86 eV on NiP (001), with most presenting a lower $E_{B,CO}$ than Ni. More importantly, we found that $E_{B,CO}$ is strongly dependent on the coordination number of surface adsorption sites. The average $E_{B,CO}$ of singly coordinated CO molecules over NiP_x is -1.21 ± 0.27 eV, which is much lower than that of the multi-coordinated CO adsorption being -1.91 ± 0.14 eV. Indeed, P primarily acts to reduce the CO binding strength by acting as a temperature stable means of breaking up multi-coordinated binding sites to leave singly coordinated binding sites as the remaining option. Experimentally, this was demonstrated by the appearance and dominance of atop site (singly coordinated) in the infrared at 2071 cm^{-1} on the NiP_x rather than the multi-coordinated CO at 1845 cm^{-1} (computed infrared frequency is shown in **Table S2**). Moreover, the improvement of CO selectivity with the second P incorporation step, which would further break up the Ni multi-binding sites, is consistent with this conclusion.

CONCLUSION

In summary, we report a full description of the surface evolution of colloidal Ni nanoparticles under the CO_2 hydrogenation conditions, by combining the AP-XPS and complementary *operando* spectroscopic and microscopic probes. The mono-layer phosphine ligands encapsulating Ni nanoparticles results in P incorporation in the real catalyst at the elevated temperature, which diffuses into the interior of the nanoparticles under oxidative gas atmosphere, leaving a NiO surface, and returns the nanoparticle surface to form NiP_x under reductive CO_2 hydrogenation conditions. Such a ligand-induced surface evolution is responsible for the significantly improved selectivity to CO production owing to the decreased *CO adsorption strength over the NiP_x surface, while amine-capped Ni remains a CO_2 methanation catalyst. Furthermore, the secondary P modification drives the complete phosphorization of NiO (under oxidative atmosphere) and metallic Ni (under reductive atmosphere) surface sites, which generates a catalyst with a 100% CO selectivity in CO_2 hydrogenation. Given the fact that phosphine is one of the most representative surfactants in the colloidal nanoparticle library, we anticipate that the P diffusion and incorporation effect will likely modulate many other nanoparticle catalyst properties, providing a new controlling knob for governing reaction that are critical to energy and environmental sustainability.

ASSOCIATED CONTENT

Supporting Information

The supporting information is available free of charge at http://pubs.acs.org. Experimental section and Figures S1-S9.

AUTHOR INFORMATION

Corresponding Author

Yifan Ye – *National Synchrotron Radiation Laboratory, University of Science and Technology of China, Hefei, 230029, P. R. China; Advanced Light Source, Lawrence Berkeley National Laboratory, Berkeley, California 94720, USA; Chemical Sciences Division, Lawrence Berkeley National Laboratory, Berkeley, California 94720, USA;* ORCID: 0000-0003-4123-9387;
Email:yifanye92@ustc.edu.cn

Zhangxiong Wu – *School of Chemical and Environmental Engineering, College of Chemistry, Chemical Engineering and Materials Science, Soochow University, Suzhou, Jiangsu 2151213, P. R. China*; ORCID: 0000-0002-2899-6474;
Email: zhangwu@suda.edu.cn

Sen Zhang – Department of Chemistry, University of Virginia, Charlottesville, Virginia 22904, USA; ORCID: 0000-0002-1716-3741;
Email: sz3t@virginia.edu

Author

Xiangru Wei – Department of Chemistry, University of Virginia, Charlottesville, Virginia 22904, USA; School of Chemical and Environmental Engineering, College of Chemistry, Chemical Engineering and Materials Science, Soochow University, Suzhou, Jiangsu 2151213, P. R. China; Department of Chemical Engineering, University of Virginia, Charlottesville, Virginia 22904, USA

Grayson Johnson – Department of Chemistry, University of Virginia, Charlottesville, Virginia 22904, USA

Meiyang Cui – Department of Chemistry, University of Virginia, Charlottesville, Virginia 22904, USA

Shen-Wei Yu – Department of Chemistry, University of Virginia, Charlottesville, Virginia 22904, USA

Yihua Ran – School of Physical Science and Technology, Shanghai Tech University, Shanghai 201210, P. R. China

Jun Cai – School of Physical Science and Technology, ShanghaiTech University, Shanghai 201210, P. R. China

Zhi Liu – School of Physical Science and Technology, ShanghaiTech University, Shanghai 201210, P. R. China

Xi Chen – Department of Materials Science and Engineering, North Carolina State University, Raleigh, North Carolina 27601, USA

Wenpei Gao – Department of Materials Science and Engineering, North Carolina State University, Raleigh, North Carolina 27601, USA

Ethan J. Crumlin – Advanced Light Source, Lawrence Berkeley National Laboratory, Berkeley, California 94720, USA; Chemical Sciences Division, Lawrence Berkeley National Laboratory, Berkeley, California 94720, USA

Xu Zhang − Department of Physics and Astronomy, California State University Northridge, Northridge, California 91330, USA
Robert J. Davis − Department of Chemical Engineering, University of Virginia, Charlottesville, Virginia 22904, USA

Notes

The authors declare no competing interest.

ACKNOWLEDGMENT

This work was supported by the University of Virginia Faculty Start-up Fund and 4-VA collaborative research program. This research used resources of the Advanced Light Source, which is a DOE Office of Science User Facility, under contract no. DE-AC02-05CH11231. Y.Y. and E.J.C. were partially supported by an Early Career Award in the Condensed Phase and Interfacial Molecular Science Program, in the Chemical Sciences Geosciences and Biosciences Division of the Office of Basic Energy Sciences of the U.S. Department of Energy, under Contract No. DE-AC02-05CH11231. Part of this research used the lab-based APXPS, which is supported by ME2 project under contract no. 11227902 from National Natural Science Foundation of China. Z.W. acknowledges the support from the National Natural Science Foundation of China (21875153). X.W. acknowledges the fellowship from the China Scholarships Council. The electron microscopy was performed in part at the Analytical Instrumentation Facility (AIF) at North Carolina State University, which is supported by the State of North Carolina and the National Science Foundation (ECCS-2025064). The AIF is a member of the North Carolina Research Triangle Nanotechnology Network (RTNN), a site in the National Nanotechnology Coordinated Infrastructure (NNCI). Y.Y. acknowledge the support from National Natural Science Foundation of China (22172153), Users with Excellence Program of Hefei Science Center CAS (2021HSC-UE001), and the support from University of Science and Technology of China (USTC).

REFERENCES

(1) Lashof, D. A.; Ahuja, D. R. Relative contributions of greenhouse gas emissions to global warming. *Nature* **1990**, *344*, 529-531.
(2)Artz, J.; Müller, T. E.; Thenert, K.; Kleinekorte, J.; Meys, R.; Sternberg, A.; Bardow, A.; Leitner, W. Sustainable Conversion of Carbon Dioxide: An Integrated Review of Catalysis and Life Cycle Assessment. *Chem. Rev.* **2018**, *118*, 434-504.
(3) Aresta, M.; Dibenedetto, A.; Angelini, A. Catalysis for the valorization of exhaust carbon: from CO_2 to chemicals, materials, and fuels. technological use of CO_2. *Chem. Rev.* **2014**, *114*, 1709-1742.
(4) Tackett, B. M.; Gomez, E.; Chen, J. G. Net reduction of CO2 via its thermocatalytic and electrocatalytic transformation reactions in standard and hybrid processes. *Nat. Catal.* **2019**, *2*, 381-386.
(5) De, S.; Dokania, A.; Ramirez, A.; Gascon, J. Advances in the Design of Heterogeneous Catalysts and Thermocatalytic Processes for CO_2 Utilization. *ACS Catal.* **2020**, *10*, 14147-14185.
(6) Ra, E. C.; Kim, K. Y.; Kim, E. H.; Lee, H.; An, K.; Lee, J. S. Recycling Carbon Dioxide through Catalytic Hydrogenation: Recent Key Developments and Perspectives. *ACS Catal.* **2020**, *10*, 11318-11345.
(7) Wang, Y. N.; Winter, L. R.; Chen, J. G. G.; Yan, B. H. CO_2 hydrogenation over heterogeneous catalysts at atmospheric pressure: from electronic properties to product selectivity. *Green Chemistry* **2021**, *23*, 249-267.
(8) Navarro-Jaén, S.; Virginie, M.; Bonin, J.; Robert, M.; Wojcieszak, R.; Khodakov, A. Y. Highlights and challenges in the selective reduction of carbon dioxide to methanol. *Nat. Rev. Chem.* **2021**, *5*, 564-579.
(9) Nielsen, D. U.; Hu, X.-M.; Daasbjerg, K.; Skrydstrup, T. Chemically and electrochemically catalysed conversion of CO2 to CO with follow-up utilization to value-added chemicals. *Nat. Catal.* **2018**, *1*, 244-254.
(10) Kattel, S.; Liu, P.; Chen, J. G. Tuning Selectivity of CO2 Hydrogenation Reactions at the Metal/Oxide Interface. *J. Am. Chem. Soc.* **2017**, *139*, 9739-9754.
(11) Vogt, C.; Groeneveld, E.; Kamsma, G.; Nachtegaal, M.; Lu, L.; Kiely, C. J.; Berben, P. H.; Meirer, F.; Weckhuysen, B. M. Unravelling structure sensitivity in CO_2 hydrogenation over nickel. *Nat. Catal.* **2018**, *1*, 127-134.
(12) Wang, Y.; Winter, L. R.; Chen, J. G.; Yan, B. CO_2 hydrogenation over heterogeneous catalysts at atmospheric pressure: from electronic properties to product selectivity. *Green Chem.* **2021**, *23*, 249-267.
(13) Zhang, J.; Deo, S.; Janik, M. J.; Medlin, J. W. Control of Molecular Bonding Strength on Metal Catalysts with Organic Monolayers for CO_2 Reduction. *J. Am. Chem. Soc.* **2020**, *142*, 5184-5193.
(14) Frei, M. S.; Mondelli, C.; García-Muelas, R.; Morales-Vidal, J.; Philipp, M.; Safonova, O. V.; López, N.; Stewart, J. A.; Ferré, D. C.; Pérez-Ramírez, J. Nanostructure of nickel-promoted indium oxide catalysts drives selectivity in CO_2 hydrogenation. *Nat. Commun.* **2021**, *12*, 1960.
(15) Aitbekova, A.; Wu, L. H.; Wrasman, C. J.; Boubnov, A.; Hoffman, A. S.; Goodman, E. D.; Bare, S. R.; Cargnello, M. Low-Temperature Restructuring of CeO_2-Supported Ru Nanoparticles Determines Selectivity in CO_2 Catalytic Reduction. *J. Am. Chem. Soc.* **2018**, *140*, 13736-13745.
(16) Wang, L. X.; Guan, E. J.; Wang, Z. Q.; Wang, L.; Gong, Z. M.; Cui, Y.; Yang, Z. Y.; Wang, C. T.; Zhang, J.; Meng, X. J.; Hu, P. J.; Gong, X. Q.; Gates, B. C.; Xiao, F. S. Dispersed Nickel Boosts Catalysis by Copper in CO_2 Hydrogenation. *ACS Catal.* **2020**, *10*, 9261-9270.
(17) Yan, B.; Zhao, B.; Kattel, S.; Wu, Q.; Yao, S.; Su, D.; Chen, J. G. Tuning CO_2 hydrogenation selectivity via metal-oxide interfacial sites. *J. Catal.* **2019**, *374*, 60-71.
(18) Matsubu, J. C.; Zhang, S.; DeRita, L.; Marinkovic, N. S.; Chen, J. G.; Graham, G. W.; Pan, X.; Christopher, P. Adsorbate-mediated strong metal–support interactions in oxide-supported Rh catalysts. *Nat. Chem.* **2017**, *9*, 120-127.
(19) Parastaev, A.; Muravev, V.; Huertas Osta, E.; van Hoof, A. J. F.; Kimpel, T. F.; Kosinov, N.; Hensen, E. J. M. Boosting CO_2 hydrogenation via size-dependent metal–support interactions in cobalt/ceria-based catalysts. *Nat. Catal.* **2020**, *3*, 526-533.
(20) Li, X. Y.; Lin, J.; Li, L.; Huang, Y. K.; Pan, X. L.; Collins, S. E.; Ren, Y. J.; Su, Y.; Kang, L. L.; Liu, X. Y.; Zhou, Y. L.; Wang, H.; Wang, A. Q.; Qiao, B. T.; Wang, X. D.; Zhang, T. Controlling CO_2 Hydrogenation Selectivity by Metal-Supported Electron Transfer. *Angew. Chem. Int. Ed.* **2020**, 8.
(21) Yang, S.-C.; Pang, S. H.; Sulmonetti, T. P.; Su, W.-N.; Lee, J.-F.; Hwang, B.-J.; Jones, C. W. Synergy between Ceria Oxygen Vacancies and Cu Nanoparticles Facilitates the Catalytic Conversion of CO_2 to CO under Mild Conditions. *ACS Catal.* **2018**, *8*, 12056-12066.
(22) Kwak, J. H.; Kovarik, L.; Szanyi, J. Heterogeneous Catalysis on Atomically Dispersed Supported Metals: CO_2 Reduction on Multifunctional Pd Catalysts. *ACS Catal.* **2013**, *3*, 2094-2100.
(23) Nelson, N. C.; Chen, L. X.; Meira, D.; Kovarik, L.; Szanyi, J. In Situ Dispersion of Palladium on TiO_2 During Reverse Water-Gas Shift Reaction: Formation of Atomically Dispersed Palladium. *Angew. Chem. Int. Ed.* **2020**, *132*, 17810-17816..
(24) Wang, Y.; Zhang, C.; Wang, X.; Guo, J.; Sun, Z.-M.; Zhang, H. Site-Selective CO_2 Reduction over Highly Dispersed Ru-SnO^x Sites Derived from a $[Ru@Sn_9]^{6-}$ Zintl Cluster. *ACS Catal.* **2020**, *10*, 7808-7819.
(25) Schlogl, R. Heterogeneous catalysis. *Angew. Chem. Int. Ed.* **2015**, *54*, 3465-3520.
(26) Yin, Y.; Alivisatos, A. P. Colloidal nanocrystal synthesis and the organic–inorganic interface. *Nature* **2005**, *437*, 664-670.
(27) Xia, Y.; Xiong, Y.; Lim, B.; Skrabalak, S. E. Shape-controlled synthesis of metal nanocrystals: simple chemistry meets complex physics? *Angew. Chem. Int. Ed.* **2009**, *48*, 60-103.
(28) Wang, C.; Daimon, H.; Onodera, T.; Koda, T.; Sun, S. A general approach to the size - and shape - controlled synthesis of platinum nanoparticles and their catalytic reduction of oxygen. *Angew. Chem. Int. Ed.* **2008**, *120*, 3644-3647.
(29) Chen, C.; Kang, Y.; Huo, Z.; Zhu, Z.; Huang, W.; Xin, H. L.; Snyder, J. D.; Li, D.; Herron, J. A.; Mavrikakis, M.; Chi, M.; More, K. L.; Li, Y.; Markovic, N. M.; Somorjai, G. A.; Yang, P.; Stamenkovic, V. R. Highly crystalline multimetallic nanoframes with three-dimensional electrocatalytic surfaces. *Science* **2014**, *343*, 1339-1343.
(30) Cargnello, M. Colloidal nanocrystals as building blocks for well-defined heterogeneous catalysts. *Chem. Mater.* **2019**, *31*, 576-596.
(31) Liu, C.; Qian, J.; Ye, Y.; Zhou, H.; Sun, C.-J.; Sheehan, C.; Zhang, Z.; Wan, G.; Liu, Y.-S.; Guo, J.; Li, S.; Shin, H.; Hwang, S.; Gunnoe, T. B.; Goddard, W. A.; Zhang, S. Oxygen evolution reaction over catalytic

single-site Co in a well-defined brookite TiO2 nanorod surface. *Nature Catalysis* **2021**, *4*, 36-45.
(32) Wu, C. H.; Liu, C.; Su, D.; Xin, H. L.; Fang, H.-T.; Eren, B.; Zhang, S.; Murray, C. B.; Salmeron, M. B. Bimetallic synergy in cobalt–palladium nanocatalysts for CO oxidation. *Nature Catalysis* **2019**, *2*, 78-85.
(33) Aziz, M. A. A.; Jalil, A. A.; Triwahyono, S.; Ahmad, A. CO2 methanation over heterogeneous catalysts: recent progress and future prospects. *Green Chemistry* **2015**, *17*, 2647-2663.
(34) Zhang, S.; Hao, Y.; Su, D.; Doan-Nguyen, V. V.; Wu, Y.; Li, J.; Sun, S.; Murray, C. B. Monodisperse core/shell Ni/FePt nanoparticles and their conversion to Ni/Pt to catalyze oxygen reduction. *J Am Chem Soc* **2014**, *136*, 15921-15924.
(35) Metin, O.; Mazumder, V.; Ozkar, S.; Sun, S. S. Monodisperse Nickel Nanoparticles; and Their Catalysis in Hydrolytic Dehydrogenation of Ammonia Borane. *Journal of the American Chemical Society* **2010**, *132*, 1468-+.
(36) Yan, X.; Sun, W.; Fan, L.; Duchesne, P. N.; Wang, W.; Kübel, C.; Wang, D.; Kumar, S. G. H.; Li, Y. F.; Tavasoli, A.; Wood, T. E.; Hung, D. L. H.; Wan, L.; Wang, L.; Song, R.; Guo, J.; Gourevich, I.; Jelle, A. A.; Lu, J.; Li, R.; Hatton, B. D.; Ozin, G. A. Nickel@Siloxene catalytic nanosheets for high-performance CO_2 methanation. *Nature Communications* **2019**, *10*, 2608.
(37) Muroyama, H.; Tsuda, Y.; Asakoshi, T.; Masitah, H.; Okanishi, T.; Matsui, T.; Eguchi, K. Carbon dioxide methanation over Ni catalysts supported on various metal oxides. *Journal of Catalysis* **2016**, *343*, 178-184.
(38) Kwak, J. H.; Kovarik, L.; Szanyi, J. CO2 Reduction on Supported Ru/Al2O3 Catalysts: Cluster Size Dependence of Product Selectivity. *ACS Catal.* **2013**, *3*, 2449-2455.
(39) Nesbitt, H. W.; Legrand, D.; Bancroft, G. M. Interpretation of Ni2p XPS spectra of Ni conductors and Ni insulators. *Phys. Chem. Miner.* **2000**, *27*, 357-366.
(40) You, B.; Jiang, N.; Sheng, M. L.; Bhushan, M. W.; Sun, Y. J. Hierarchically Porous Urchin-Like Ni2P Superstructures Supported on Nickel Foam as Efficient Bifunctional Electrocatalysts for Overall Water Splitting. *ACS Catal.* **2016**, *6*, 714-721.
(41) Kaneda, G.; Murata, J.; Takeuchi, T.; Suzuki, Y.; Sanada, N.; Fukuda, Y. Adsorption and decomposition of triethylphosphine (TEP) and tertiarybutylphosphine (TBP) on Si(001) studied by XPS, HREELS, and TPD. *Appl. Surf. Sci.* **1997**, *113-114*, 546-550.
(42) Heine, C.; Lechner, B. A. J.; Bluhm, H.; Salmeron, M. Recycling of CO_2: probing the chemical state of the Ni(111) surface during the methanation reaction with ambient-pressure X-ray photoelectron spectroscopy. *J. Am. Chem. Soc.* **2016**, *138*, 13246-13252.
(43) Elsener, B.; Atzei, D.; Krolikowski, A.; Rossi Albertini, V.; Sadun, C.; Caminiti, R.; Rossi, A. From chemical to structural order of electrodeposited $Ni_{22}P$ alloy: an XPS and EDXD study. *Chem. Mater.* **2004**, *16*, 4216-4225.
(44) Ledendecker, M.; Krick Calderon, S.; Papp, C.; Steinruck, H. P.; Antonietti, M.; Shalom, M. The synthesis of nanostructured Ni_5P_4 films and their use as a non-noble bifunctional electrocatalyst for full water splitting. *Angew. Chem. Int. Ed.* **2015**, *54*, 12361-12365.
(45) Millet, M. M.; Algara-Siller, G.; Wrabetz, S.; Mazheika, A.; Girgsdies, F.; Teschner, D.; Seitz, F.; Tarasov, A.; Levchenko, S. V.; Schlogl, R.; Frei, E. Ni Single Atom Catalysts for CO_2 Activation. *J. Am. Chem. Soc.* **2019**, *141*, 2451-2461.
(46) Galhardo, T. S.; Braga, A. H.; Arpini, B. H.; Szanyi, J.; Gonçalves, R. V.; Zornio, B. F.; Miranda, C. R.; Rossi, L. M. Optimizing active sites for high CO selectivity during CO_2 hydrogenation over supported nickel catalysts. *J. Am. Chem. Soc.* **2021**, *143*, 4268-4280.
(47) Liu, L.; Zhao, C.; Li, Y. Spontaneous dissociation of CO_2 to CO on defective surface of Cu(I)/TiO_2 nanoparticles at room temperature. *The Journal of Physical Chemistry C* **2012**, *116*, 7904-7912.
(48) Petrik, N. G.; Kimmel, G. A. Adsorption geometry of CO versus coverage on TiO_2(110) from s- and p-polarized infrared spectroscopy. *J. Phys. Chem. Lett.* **2012**, *3*, 3425-3430.
(49) Bengaard, H. S.; Nørskov, J. K.; Sehested, J.; Clausen, B. S.; Nielsen, L. P.; Molenbroek, A. M.; Rostrup-Nielsen, J. R. Steam Reforming and Graphite Formation on Ni Catalysts. *J. Catal.* **2002**, *209*, 365-384.
(50) Catapan, R. C.; Oliveira, A. A. M.; Chen, Y.; Vlachos, D. G. DFT Study of the Water–Gas Shift Reaction and Coke Formation on Ni(111) and Ni(211) Surfaces. *J. Phys. Chem. C.* **2012**, *116*, 20281-20291.
(51) Jelic, J.; Meyer, R. J. A density functional theory study of water gas shift over pseudomorphic monolayer alloy catalysts: Comparison with NO oxidation. *J. Catal.* **2010**, *272*, 151-157.
(52) Zhu, Y.-A.; Chen, D.; Zhou, X.-G.; Yuan, W.-K. DFT studies of dry reforming of methane on Ni catalyst. *Catal. Today.* **2009**, *148*, 260-267.

Table of Contents (TOC)